IEEE Access
Multidisciplinary | Rapid Review | Open Access Journal

Received 1 November 2022, accepted 29 November 2022, date of publication 9 December 2022,
date of current version 20 December 2022.

Digital Object Identifier 10.1109/ACCESS.2022.3227967

METHODS

Setting Method of Downsampling Factor and Grid Factor for NDT Relocation Algorithm in Dynamic Environment

JIAN GU[1,2], YUBIN LAN[1,2,3], FANXIA KONG[1,2], LEI LIU[1,2], AND LILI YI[1,2]

[1]School of Agricultural Engineering and Food Science, Shandong University of Technology, Zibo 255000, China
[2]National Sub-Center for International Collaboration Research on Precision Agricultural Aviation Pesticide Spraying Technology, Shandong University of Technology, Zibo 255000, China
[3]National Center for International Collaboration Research on Precision Agricultural Aviation Pesticides Spraying Technology, College of Engineering, South China Agricultural University, Guangzhou 510642, China

Corresponding author: Lili Yi (yili0001@sdut.edu.cn)

This work was supported in part by the Special Funding Project for "One Event and One Discussion" for Importing Top Talents in Shandong Province under Grant Lu Zheng Ban Zi [2018]27, and in part by the Zibo Unmanned Farm Research Institute Project under Grant 2019ZBXC200.

ABSTRACT Normal Distribution Transform (NDT) algorithm plays the role of detecting the relative pose of the vehicle in high-precision map. In this paper, a method of setting downsampling factor and grid factor for NDT relocation algorithm in dynamic environment is proposed, which can solve the problems of excessive NDT relocation error and location loss caused by dynamic objects accounting for 1% to 35% of the volume of scanning point cloud in vehicle environment. To simulate a real dynamic point cloud environment, the single-frame LiDAR point cloud space is voxelized into a mesh. Each grid is assigned a random number evenly distributed between 0 and 1. The threshold value for whether to add a Gaussian noise point is also set. Seven representative dynamic objects on the highway are selected. The threshold value of probability distribution function of Gaussian noise object needs to be set. Then the volume content of the dynamic object in the single frame point cloud space is calculated according to the set threshold value by using the definite integral. By changing the content and volume of dynamic obstacles in a dynamic environment, the effects of the downsampling factor and the grid factor on the accuracy of the repositioning trajectory are obtained. The resampling and mesh coefficients are optimized based on the analysis of the repositioning trajectory accuracy. The results show that When the current sampling factor is fixed, the grid factor of the NDT algorithm is proportional to the RMSE factor. When the NDT grid factor is fixed and the down sampling factor is equal to the side length of the obstacle, the NDT relocation accuracy is the highest and reaches the local optimum.

INDEX TERMS Normal distributions transform, high-precision map, dynamic point cloud environment, relocation.

I. INTRODUCTION

Relocation plays a critical role in autonomous driving related applications, such as localizing a vehicle in a known map, and maintaining the accuracy of simultaneous localization and mapping (SLAM). During the last two decades, a variety of relocation methods have achieved great success in tackling such problems using Global Positioning System (GNSS) [1], [2], [3], Inertial Measurement Unit (IMU) [4], [5], [6], camera [7], [8], LiDAR [9], [10], [11], and other perceptual sensors.

A common solution to these problems is given by Inertial Navigation Systems (INS) employing GNSS and an IMU. However, GNSS suffer from disruptions or signal loss due to obstruction of the sky caused for example by city [1]. One solution to this problem is given by using odometry information to compensate for sudden jumps in the

The associate editor coordinating the review of this manuscript and approving it for publication was Okyay Kaynak.

GNSS measurements [12], [13]. However, the performance often remains insufficient for autonomous driving related applications.

Cameras are one of the most attractive relocation sensors because of their inherent high information content, low cost, and small size. Visual relocation uses the large amount of information provided by the camera to estimate robot position [14], [15], [16], [17], [18]. Zheng [19] proposes a new visual measurement framework to achieve accurate, reliable and cost-effective vehicle positioning in semi-obscured and GPS-obscured urban environments. In most practical work, the method of visual relocation using a camera is susceptible to changes in scene illumination. In order to improve the robustness of the visual relocation to the changes of ambient illumination in the actual work, Xu [20] proposed a method of constructing multiple maps of different illumination intensities. By means of constructing multiple maps with different light intensities, a map with consistent lighting is then selected based on the current image brightness. However, for outdoor large-scale relocation, ensuring its robust operation is still very challenging especially in changing environments.

An increasingly popular solution to the problem of moving vehicle positioning in city is given by dropping GNSS and camera measurements altogether, and by relying on a LiDAR that measures 3D scans of the environment. Compared with cameras and GNSS, LiDAR has better penetrability and anti-interference characteristics. Furthermore, the amount of data acquired by a LiDAR system is less than in the case of a camera. Hence the LiDAR sensor is used frequently for positioning and object detection [21]. However, most LiDAR-based localization solutions with prior point-cloud maps [22], [23], [24], [25] assume that the road scenes are relatively constant, while new constructions, road-side vegetation, partial occlusions by changing objects may severely compromise robustness. Therefore, an interesting but open question is whether LiDAR can be used for robust relocalization in large-scale changing environments.

In this article, the dataset is used to test the accuracy of the NDT relocation system in a dynamic environment. Our main contributions are summarized as follows:

- A dynamic environment simulation and dynamic object content solution method based on Gaussian noise is presented. Single-frame point cloud voxels are gridded, and each grid is given a random number that is evenly distributed between 0 and 1. A threshold value for selecting a voxelized grid is set. The Gaussian noise point is added to the selected voxel grid. Finally, the volume content of dynamic objects in the single-frame point cloud space is calculated based on the threshold value selected by the definite integral.
- A method for calculating the number of LiDAR Points of a dynamic Gaussian noise object is presented. Seven dynamic objects with high frequency in highway environment were selected as the test target. When adults are 5m away from LiDAR, 100 LiDAR Points in disturbed point cloud space of 1 cubic meter are taken as the standard. The number of Gauss noise points added to a dynamic object is the dynamic object perturbation point cloud space volume multiplied by the number of LiDAR Points per unit point cloud space 100.
- A method for optimizing the settings of the downsampling coefficients and grid coefficients based on the NDT relocation algorithm in a dynamic environment is presented. By changing the content and volume of dynamic obstacles in a dynamic environment, the effects of the downsampling factor and the grid factor on the accuracy of the repositioning trajectory are obtained. Optimal solution of downsampling and grid coefficients using repositioning Trajectory Accuracy.

The remainder of this paper is organized as follows. Section II presents a literature review of existing studies on this topic. Section III then presents the proposed methodology. The practical experiments and the corresponding results are provided in Section IV. Finally, Section V draws some conclusions.

II. RELATED WORK

With the increasing interest in robotic technology, the construction of high-precision maps and the implementation of repositioning algorithms are being actively studied to enable automobile driving on roads.

A. SIMULTANEOUS LOCALIZATION AND MAPPING

New technologies such as machine vision and SLAM have tremendous potential in autonomous driving. SLAM is divided into two main methods: visual simultaneous localization and mapping (V-SLAM), which depends on a camera, and light detection and ranging simultaneous localization and mapping (LiDAR-SLAM), which depends on a LiDAR sensor. Visual SLAM can be divided into direct and indirect methods according to different ways of estimating camera motion. The direct method estimates camera motion by minimizing the photometric error of image pixels. SVO uses a classic sparse direct SLAM system [26]. The position estimation is performed through FAST features in the image. Because the number of estimated pixels is very small, its operation efficiency is very high.Because of the high sensitivity of the image to illumination changes, the visual SLAM system using direct methods has poor robustness. The indirect method, also known as the feature point method, estimates the camera posture by matching the feature points between images. The ORB-SLAM2 system is the most classic visual SLAM system based on the feature point method [27]. The system integrates three threads of tracking, local map, and loopback detection, which can effectively improve the running speed and pose accuracy of the system. Even though ORB-SLAM2 is very active in automatic driving. But many walls and windows in a city are made of glass or vinyl and are easily exposed to light during the day.

The LiDAR sensor not only provides centimeter level distance information, but also has a wide detection range, independent of lighting conditions [28], [29]. LiDAR Odometry and Mapping (LOAM) [30], [31], [32] is presently the most representative real-time 3D laser SLAM algorithm based on feature matching. It has a small amount of calculation and motion compensation. LOAM performs point feature to edge/plane scan-matching to find correspondences between scans. Features are extracted by calculating the roughness of a point in its local region. Real-time performance is achieved by novelly dividing the estimation problem across two individual algorithms. One algorithm runs at high frequency and estimates sensor velocity at low accuracy. The other algorithm runs at low frequency but returns high accuracy motion estimation. The two estimates are fused together to produce a single motion estimate at both high frequency and high accuracy. The mapping accuracy of LOAM in dataset is always in the forefront, and the effect is also very good in the actual environment, so it can be used to build high-precision maps, as shown in Fig.1.

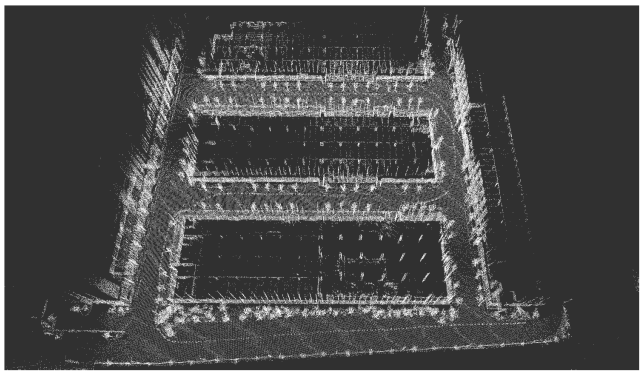

FIGURE 1. High-precision maps of real datasets.

B. RELOCATION ALGORITHM

The NDT algorithm [33], [34], [35], [36], [37] is used to relocate maps with deviations [38], [39]. Instead of comparing the difference between point clouds and points in two cities, NDT first converts a high-precision map of a city into a normal distribution of multidimensional variables. If the transformation parameters make the two LiDAR data match well, the probability density of the transformation points in the reference system will be high. Therefore, when the transformation parameters are optimized to maximize the sum of probability density, the LiDAR point cloud data of the two cities will be best matched, as shown in Fig.2.

The use of a normal distribution to represent an otherwise discrete the high-precision map has many benefits. This chunked, smooth representation is continuously derivable and the probability density function of each lattice can be thought of as an approximation to a local surface, which not only describes the location of the surface in space, but also contains information about the orientation and smoothness of the surface.

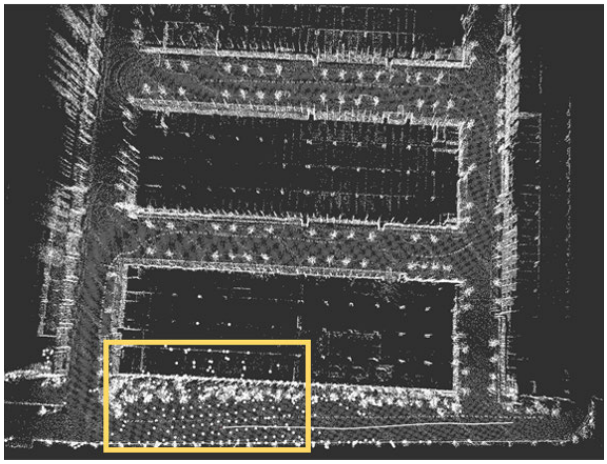

(a) Global situation map based on high-precision map relocation

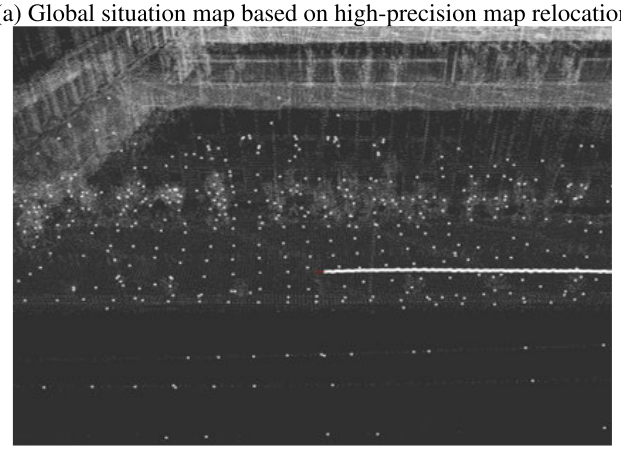

(b) Local enlargement based on high-precision map relocation

FIGURE 2. Relocation based on high-precision maps.

III. NDT RELOCATION

First, it is necessary to load the high-precision map and process the LiDAR point cloud data obtained by LiDAR scanning. Then, the LiDAR point cloud data is divided into voxel grids. Gaussian noise is added to the obtained random voxel grids to simulate real obstacles. Finally, the simulated point cloud with added Gaussian noise is voxel down sampled as the input point cloud of NDT relocation algorithm. The specific steps are shown in Fig.3.

A. PROBLEM DESCRIPTION

Relocation loss or low accuracy due to uncertainty in the size and number of point cloud objects in a dynamic point cloud environment. Therefore, the low error NDT location in dynamic environment is a big challenge. Downsampling coefficient and grid coefficient have a great relationship with the relocation accuracy. Set the function relationship between the downsampling factor a and the NDT relocation error to be $f_D(a)$, The function relationship between the grid factor b and the NDT relocation error in the NDT relocation algorithm is $f_N(b)$, so the function relationship between the NDT relocation error and the grid factor B in the downsampling factor A and the NDT relocation algorithm is

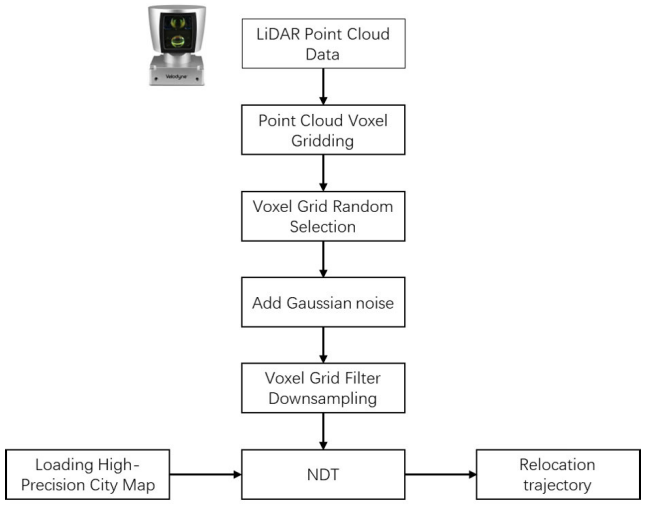

FIGURE 3. NDT relocation flow chart.

$F[f_D(a), f_N(b)]$. So the minimum error formula we need to get for NDT is:

$$[f_D(a), f_N(b)]^* = \underset{[f_D(a), f_N(b)]}{\arg\min} F[f_D(a), f_N(b)] \quad (1)$$

B. DYNAMIC POINT CLOUD ENVIRONMENT SIMULATION

In order to obtain voxel grids at random locations, give each square a random number λ_i is evenly distributed between [0,1], i is the ordinal number of the voxel grid in single-frame point cloud space, $H(\lambda_i)$ is the function relationship of adding Gaussian noise to the single voxel grid. z is the threshold value that directly affects the probability value P of adding noise, ranging from 0 to 1, then the function formula of generating a Gaussian noise barrier is:

$$H(\lambda_i) = \begin{cases} 0 & (\lambda_i > z) \\ 1 & (\lambda_i \le z). \end{cases} \quad (2)$$

$f_P(x)'$ is the probability density function of adding Gaussian noise to each grid. Then the probability of each lattice adding noise to become a noise lattice is P, and the formula is:

$$P = \int_0^z f_P(x)' dx. \quad (3)$$

The location of each voxel grid obtained is random. In order to obtain the maximum capacity of the algorithm for dynamic obstacles of different volumes, the size of voxel grid probability n can be specified. After obtaining the random voxel grid, the Gaussian noise is added to the obtained voxel grid [40], [41], [42], [43], [44], [45]. The calculation method can be easily obtained by using the knowledge of normal distribution in probability theory. The probability density of Gaussian noise obeys the Gaussian distribution [46], [47], [48], and the formula of the Gaussian distribution is:

$$f(x) = \frac{1}{\sqrt{2\pi}\sigma} \exp\left(-\frac{(x-\mu)^2}{2\sigma^2}\right). \quad (4)$$

(a) Tracked vehicles equipped with LiDAR

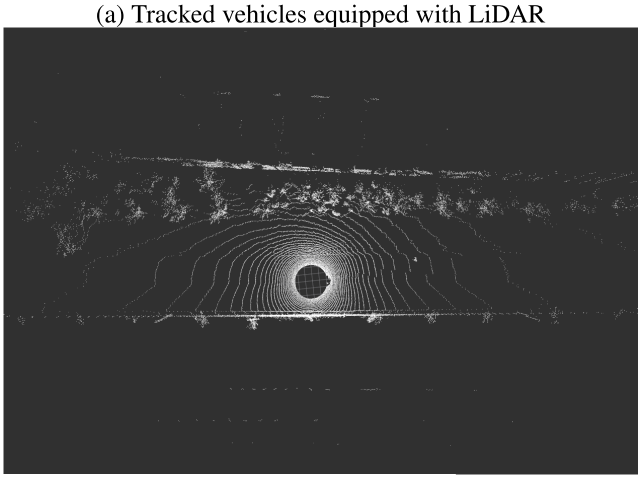

(b) Original LiDAR data

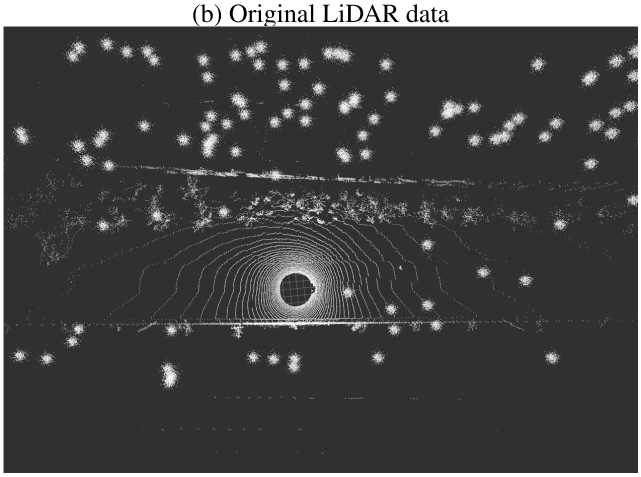

(c) LiDAR data with Gaussian noise

FIGURE 4. Dynamic environment simulation.

Here μ is the mean value of the voxel grid taken, and the value of σ is a quarter of the voxel grid. The number of noise points for each grid is calculated according to the actual situation.

Based on the size of point cloud space disturbed by objects in the real dynamic environment, the spatial volume of point

Algorithm 1 Dynamic Point Cloud Environment Simulation

Input: Give each square a random number λ_i; i is the ordinal number of the voxel grid in single-frame point cloud space; z is the threshold value, [0,1]; $f_P(x)'$ is the probability density function of adding Gaussian noise to each grid

Output: P,H (λ_i)

1: Extracting the set of reliable negative and/or positive samples T_n from U_n with help of P_n;
2: Voxel meshing of LIDAR point cloud data;
3: Input threshold $z \in [0, 1]$;
4: Calculate the probability P of each grid becoming a noise grid;
5: Input each $\lambda_i \in [0, 1]$;
6: If $\lambda_i > z$, $H(\lambda_i) = 0$, else $H(\lambda_i) = 1$

TABLE 1. Parameters of adding noise to 7 common objects on urban roads.

	Volume/m³	Noise points/pcs	voxel side length/m	distance/m
Pet	1	100	1	5
Adults	2	200	1.26	5
Man and car	5	500	1.71	5
Small car	15	1500	2.47	5
Small truck	30	3000	3.11	5
Medium truck A	45	4500	3.56	5
Medium truck B	60	6000	3.91	5

cloud disturbed by common objects on the road is calculated. According to the safety requirements of highways, the safe distance between pedestrians and vehicles is larger than 3m. The average distance between the writer and the LiDAR is set to 5m. At this time, the number of LiDAR points constituting adults is about 200. The space volume of Adult Normal perturbation point cloud is about $2m^3$. Therefore, $1m^3$ the number of additional LiDAR noise points in the volume point cloud space is set to 100. Data for other common objects on roads is shown in Table1.

C. VOXEL DOWNSAMPLING

The more dense the input point cloud points, the more computational complexity is required for NDT registration. Autopilot LiDAR positioning has higher real-time requirements. The less time it takes for point cloud registration, the better. Therefore, we can improve the speed of NDT registration by downsampling the input point cloud. To avoid the overlap between the added obstacle volume and the downsampling grid, only LiDAR point clouds within 60m are retained. In each voxel grid, the center of gravity of the voxel grid is used instead of all points in the voxel to display the other points in the voxel. So that all points in the voxel are represented by a single center of gravity. As shown in Fig. 5. As a result, the number of points is reduced, the matching speed is improved, the shape characteristics of the point cloud remain basically unchanged, and the spatial structure information is preserved. The larger the voxel raster selection, the fewer point clouds sampled, and the faster the processing speed. However, the original point cloud will be too fuzzy,

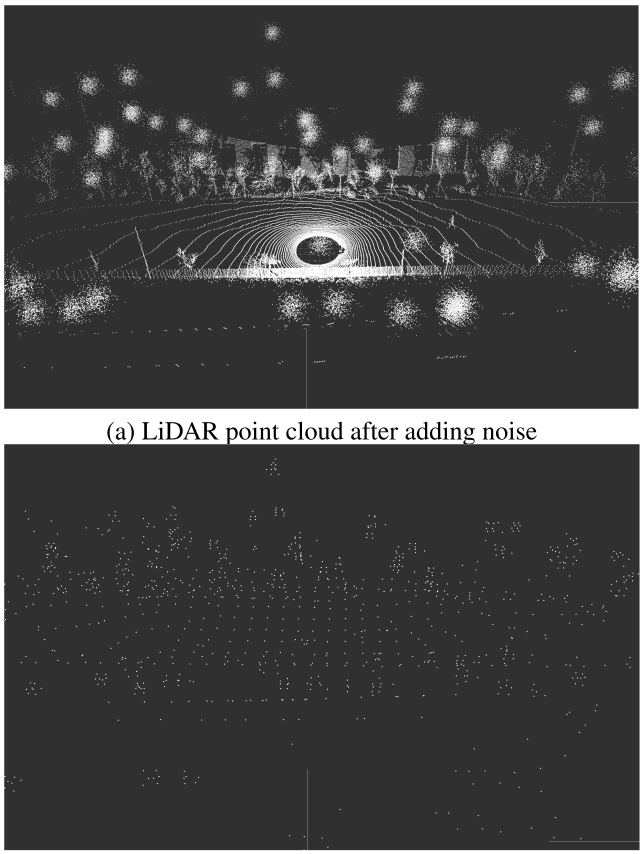

(a) LiDAR point cloud after adding noise

(b) LiDAR point cloud after downsampling

FIGURE 5. Dynamic LiDAR point cloud data downsampling.

and the smaller the voxel raster selection, the opposite effect will be achieved [49], [50], [51], [52].

D. NDT RELOCATION ALGORITHMS

The first step is to grid 3D high-precision map point cloud. The cube is used to divide the entire space of the LiDAR points. Finally, the probability density function for each grid is calculated based on the points in the grid.

$$\vec{\mu} = \frac{1}{m}\sum_{k=1}^{m}\vec{y}_k \tag{5}$$

$$\Sigma = \frac{1}{m}\sum_{k=1}^{m}(\vec{y}_k - \vec{\mu})(\vec{y}_k - \vec{\mu})^T \tag{6}$$

where $\vec{\mu}$ is the mean of the normal distribution of the grids of the high-precision map, m indicates the number of points in the high-precision map grid, k means the kth point in the high-precision map grid, $\vec{y}_{k=1,\ldots,m}$ for all scanned points in a high-precision map grid, Σ denotes the covariance matrix of the high-precision map grid, The probability density function of a grid can be described as

$$f(\vec{x}) = \frac{1}{(2\pi)^{\frac{3}{2}}\sqrt{|\Sigma|}} e^{-\frac{(\vec{x}-\vec{\mu})^T\Sigma^{-1}(\vec{x}-\vec{\mu})}{2}}. \tag{7}$$

The use of a normal distribution to represent an otherwise discrete the high-precision map has many benefits. This chunked, smooth representation is continuously derivable and the probability density function of each lattice can be thought of as an approximation to a local surface, which not only describes the location of the surface in space, but also contains information about the orientation and smoothness of the surface.

When using NDT registration, the goal is to find the pose of the current LiDAR scan in such a way as to maximize the likelihood that the currently scanned points lie on the surface of the high-precision map. The parameter we then need to optimize is the transformation (rotation, translation, etc.) of the currently scanned LiDAR point cloud, which we describe using a transformation parameter $\vec{p}$. The current scan is a point cloud $X = \{\vec{x}_1, \ldots, \vec{x}_n\}$, given the set of scan points $X$and the transformation parameter $\vec{p}$, such that the spatial transformation function $T(\vec{p}, \vec{x}_k)$denotes the use of the pose transformation $\vec{p}$ to move the points $\vec{x}_k$,combined with the previous set of density-of-state functions (one PDF for each grid), then the best transformation parameter $\vec{p}$ should be the pose transformation that maximizes the likelihood function:

$$Likelihood : \Theta = \prod_{k=1}^{n} f\left(T\left(\vec{p}, \vec{x}_k\right)\right). \tag{8}$$

Then maximizing the likelihood is also equivalent to minimizing the negative log-likelihood $-\log\Theta$:

$$-\log\Theta = -\sum_{k=1}^{n} \log\left(f\left(T\left(\vec{p}, \vec{x}_k\right)\right)\right). \tag{9}$$

Then there is the optimization section. An optimization algorithm is used to tune the transformation parameter $\vec{p}$ to minimize this negative log likelihood. The NDT algorithm uses Newton's method for parameter optimization. Here the probability density function $f(\vec{x})$ does not have to be normally distributed; any probability density function that reflects the structural information of the scanned surface and is robust to anomalous scan points will do.

IV. EXPERIMENT

A. DATA ANALYSIS

In order to test the robustness of the NDT relocation algorithm in a dynamic environment, we used dynamic environment dataset set with a total length of 486.750m and a duration of 310s.

To explore the effects of the mesh and downsampling coefficients of the NDT algorithm on the repositioning accuracy in a dynamic environment and under what conditions can the repositioning accuracy be highest. The transformation epsilon is 0.05, the step size is 0.1, and the maximum iterations is 30. The repositioned root mean square error data is used as a measure of accuracy. As shown in Fig. 6.

Fixed downsampling factor is needed to study the effect of the grid factor of NDT algorithm on the repositioning accuracy. Normally, 16-line LiDAR uses a down-sampling factor

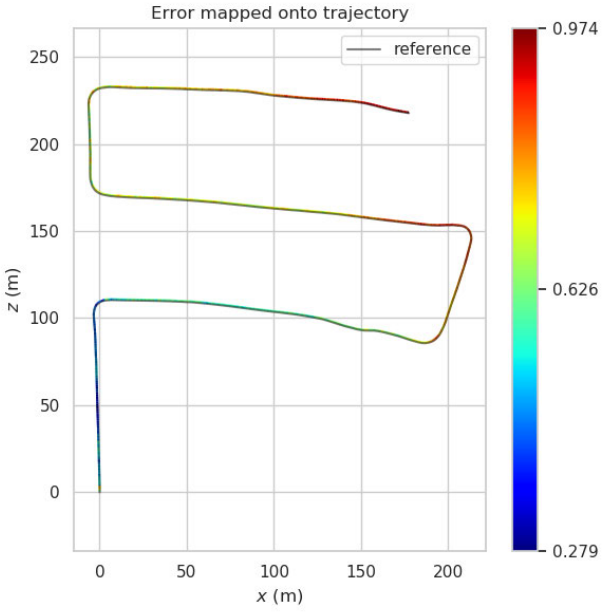

FIGURE 6. Comparison between dynamic environment dataset relocation trajectory and real trajectory with sampling factor 3.0 and grid factor 1 of NDT algorithm.

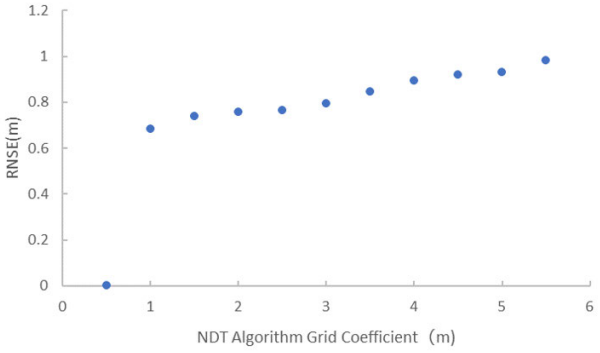

FIGURE 7. When the downsampling factor is 3.0, the influence of grid factors of different NDT algorithms on the relocation accuracy in dynamic environment data.

of 1 m to 2 m, and 32-line LiDAR uses a down-sampling factor of 2 m to 3 m. The LiDAR used in this paper is 64-line LiDAR with a sampling factor of 3.0. As an example, the noise-added voxel grid is set to 2.47m, the content is set to 0.07, and the grid factor of NDT algorithm is 0.5m per interval.

As shown in Fig. 7, it can be seen from the figure that when the downsampling coefficient is fixed, the grid coefficient is proportional to the RMSE value. The larger the grid coefficient, the lower the accuracy. When the grid coefficient of the NDT algorithm is too small, the NDT algorithm cannot relocate, because the LiDAR point cloud data is played at 10hz speed, and the real-time performance cannot be met when the grid coefficient is too small. Therefore, in order to meet the real-time requirements, the grid coefficient needs

TABLE 2. Testing the limit content and RMSE value of common objects in dynamic environment dataset.

	Failed groups/times	successful groups/times	Limit content/%	Average RMSE(m)
Pet	12	88	35	0.612455
Adults	16	84	13	0.707939
Man and car	13	87	11	0.645663
Small car	13	87	7	0.642179
27	13	87	5	0.554545
Small truck	16	84	4	0.636066
Medium truck A	19	81	3	0.646377
Medium truck B	21	79	2	0.612084

to be increased, but when the grid coefficient is too high, the relocation accuracy will be affected. Therefore, in a dynamic environment, the grid coefficient should be as small as possible. The experimental results show that when the sampling factor is 3.0 and the unit is 0.5, the lowest grid factor of the NDT algorithm is 1 while the robustness of the algorithm is guaranteed.

In order to explore the relationship between the downsampling factor and the repositioning accuracy in the real environment, the repositioning accuracy can reach the highest when the downsampling factor is chosen. The transformation epsilon is 0.05, the step size is 0.1, the resolution is 1.0, and the maximum iterations is 30. 10 sets of limit content tests were performed on each volume dynamic target, with the average root square error value of successful repositioning as the final result to reduce the risk. As shown in Table2.

In the dynamic environment, the larger the unit dynamic object volume, the greater the impact on the NDT relocation algorithm, and the smaller the capacity in the dynamic environment, so the smaller the limit content of dynamic objects. In the process of testing the limit content of dynamic objects, the number of times that the limit content of a single large dynamic object loses its location is more than that of a single small dynamic object.

In the NDT relocation algorithm, the grid is set to 3m. When the volume is between 0 m^3 and 5 m^3, the limit error increases gradually. Because the volume of a single dynamic object is small, but the number is large and dispersed, the influence on the NDT relocation algorithm is increasing. As the volume of the dynamic object increases, the limit precision of the NDT repositioning algorithm increases from 5 m^3 to 27 m^3, and the effect on the positioning accuracy decreases because the number is too small. When the volume of a dynamic object is between 27 m^3 and 60 m^3, the positioning accuracy decreases because the volume of a unit object is too large to have a greater impact on the environment.

As shown in Table3, it is found that when the edge length of the object in dynamic environment is 3 and equal to the downsampling factor, the root mean square error is the smallest and the accuracy is the highest. In order to explore the relationship between the downsampling factor and the repositioning accuracy in the real environment, and to determine the value of the downsampling factor, the repositioning accuracy can be the highest, as well as the influence of the downsampling factor and the NDT grid factor on different size obstacles. Because the downsampling factor

TABLE 3. Test data for common objects in dynamic environment dataset.

	1 (m)	1.26 (m)	1.71(m)	2.47 (m)	3(m)	3.11 (m)	3.56(m)	3.91(m)
Pet	0.608624	0.561814	0.651455	0.725890	0.625483	0.639181	0.652722	0.690330
Adults	0.643110	0.531103	0.711688	0.705359	0.732058	0.693259	0.712759	0.695845
Man and car	0.647109	0.654102	0.645360	0.731050	0.697727	0.741055	0.675921	0.818623
Small car	0.642579	0.593136	0.671121	0.659958	0.739513	0.746893	0.688389	0.640085
27	0.668267	0.721858	0.686290	0.769471	0.585952	0.663751	0.694065	0.637940
Small truck	0.719439	0.771402	0.682667	0.677633	0.681421	0.622339	0.721126	0.790851
Medium truck A	0.733336	0.556974	0.846580	0.637894	0.725888	0.652753	0.636211	0.651734
Medium truck B	0.741660	0.794250	0.720362	0.770319	0.717039	0.649923	0.650088	0.620059

TABLE 4. Test data for common objects in dynamic environment dataset.

	Downsampling factor(m)	NDT Limit Factor(m)	Limit content(%)	Average RMSE(m)
Pet	1	1.5	35	0.608624
Adults	1.26	1.5	13	0.531103
Man and car	1.71	1.5	11	0.645360
Small car	2.47	1.5	7	0.659958
27	3	1.5	5	0.554545
Small truck	3.11	1	4	0.621794
Medium truck A	3.56	1	3	0.613613
Medium truck B	3.91	1	2	0.612939

range is small when the NDT grid factor is 1.0. The NDT mesh factor is set to 1.5. Using the limit content of obstacles in the dynamic environment, the average RMSE is calculated when the downsampling factor is the barrier edge length value.

From the above experiments, it can be found that when the grid factor of NDT algorithm is fixed, there is no significant relationship between the downsampling factor and the repositioning accuracy. However, when the downsampling factor is constant and the edge length of the obstacle that appears most frequently in the dynamic environment is equal to the downsampling factor, the accuracy of relocation in this environment is the highest in many different environments. Thus, a local optimal result can be obtained.

In combination with the above experimental results, the downsampling factor is set to the edge length of the obstacle with the highest frequency in dynamic environment. The convergence law is used to minimize the NDT grid factor to obtain an appropriate factor. Finally, the average RMSE value is calculated. As shown in table 4.

When the downsampling factor is equal to the maximum obstacle edge length value in the dynamic environment and the NDT grid factor is the smallest, the redefinition accuracy is the highest, reaching the local optimum.

V. CONCLUSION

This paper solves the problem of excessive NDT relocation error and relocation loss caused by the random occurrence of dynamic objects accounting for 1% to 35% of the scanning point cloud volume in the vehicle environment. A calibration method of down sampling coefficient and grid coefficient based on NDT relocation algorithm in dynamic environment is proposed. To simulate a real dynamic point cloud environment, single-frame LiDAR point cloud spatial voxels are gridded. Each grid is given a random number that is evenly distributed between 0 and 1. The threshold value for adding Gaussian noise points to the selected voxelized grid is set. Seven representative dynamic objects on the highway are selected. The number of Gaussian noise points needed to

be added for each dynamic object is obtained by multiplying the space volume of point cloud disturbed by the dynamic object in the real dynamic environment by the number of Gaussian noise points needed to be added per unit volume. Then the volume content of the dynamic object in the single frame point cloud space is calculated according to the set threshold value by using the definite integral. By changing the content and volume of dynamic obstacles in a dynamic environment, the effects of the downsampling factor and the grid factor on the accuracy of the repositioning trajectory are obtained. When the current sampling factor is fixed, the grid factor of the NDT algorithm is inversely proportional to the RMSE factor. The smaller the NDT grid factor, the higher the accuracy in the dynamic environment. When the NDT grid factor is fixed and the downsampling factor is equal to the side length of the obstacle, the NDT relocation accuracy is the highest and reaches the local optimum. In the dynamic environment, it is recommended that the sampling coefficient should be equal to the length of the obstacle side, and then the NDT grid coefficient should be as small as possible. It can effectively improve the positioning accuracy.

REFERENCES

[1] G. He, X. Yuan, Y. Zhuang, and H. Hu, "An integrated GNSS/LiDAR-SLAM pose estimation framework for large-scale map building in partially GNSS-denied environments," *IEEE Trans. Instrum. Meas.*, vol. 70, pp. 1–9, 2020.

[2] F. Ye, S. Pan, W. Gao, H. Wang, G. Liu, C. Ma, and Y. Wang, "An improved single-epoch GNSS/INS positioning method for urban canyon environment based on real-time DISB estimation," *IEEE Access*, vol. 8, pp. 227566–227578, 2020.

[3] P. Lyu, S. Bai, J. Lai, B. Wang, X. Sun, and K. Huang, "Optimal time difference-based TDCP-GPS/IMU navigation using graph optimization," *IEEE Trans. Instrum. Meas.*, vol. 70, pp. 1–10, 2021.

[4] F. Aghili and A. Salerno, "Driftless 3-D attitude determination and positioning of mobile robots by integration of IMU with two RTK GPSs," *IEEE/ASME Trans. Mechatronics*, vol. 18, no. 1, pp. 21–31, Feb. 2013.

[5] R. Takai, O. Barawid, K. Ishii, and N. Noguchi, "Development of crawler-type robot tractor based on GPS and IMU," *IFAC Proc. Volumes*, vol. 43, no. 26, pp. 151–156, 2010.

[6] R. Sun, Y. Yang, K.-W. Chiang, T.-T. Duong, K.-Y. Lin, and G.-J. Tsai, "Robust IMU/GPS/VO integration for vehicle navigation in GNSS degraded urban areas," *IEEE Sensors J.*, vol. 20, no. 17, pp. 10110–10122, Sep. 2020.

[7] X. Chen, H. Zhang, H. Lu, J. Xiao, Q. Qiu, and Y. Li, "Robust SLAM system based on monocular vision and LiDAR for robotic urban search and rescue," in *Proc. IEEE Int. Symp. Saf., Secur. Rescue Robot. (SSRR)*, Oct. 2017, pp. 41–47.

[8] A. Vu, A. Ramanandan, A. Chen, J. A. Farrell, and M. Barth, "Real-time computer vision/DGPS-aided inertial navigation system for lane-level vehicle navigation," *IEEE Trans. Intell. Transp. Syst.*, vol. 13, no. 2, pp. 899–913, Jun. 2012.

[9] Z. J. Chong, B. Qin, T. Bandyopadhyay, M. H. Ang, E. Frazzoli, and D. Rus, "Synthetic 2D LiDAR for precise vehicle localization in 3D urban environment," in *Proc. IEEE Int. Conf. Robot. Autom.*, May 2013, pp. 1554–1559.

[10] T. Gee, J. James, W. Van Der Mark, P. Delmas, and G. Gimel'farb, "LiDAR guided stereo simultaneous localization and mapping (SLAM) for UAV outdoor 3-D scene reconstruction," in *Proc. Int. Conf. Image Vis. Comput. New Zealand (IVCNZ)*, Nov. 2016, pp. 1–6.

[11] W. Hess, D. Kohler, H. Rapp, and D. Andor, "Real-time loop closure in 2D LiDAR SLAM," in *Proc. IEEE Int. Conf. Robot. Autom. (ICRA)*, May 2016, pp. 1271–1278.

[12] M. Schreiber, H. Königshof, A.-M. Hellmund, and C. Stiller, "Vehicle localization with tightly coupled GNSS and visual odometry," in *Proc. IEEE Intell. Vehicles Symp. (IV)*, Jun. 2016, pp. 858–863.

[13] K.-W. Chiang, H.-W. Chang, Y.-H. Li, G.-J. Tsai, and P.-C. Hsu, "Assessment for INS/GNSS/odometer/barometer integration in loosely-coupled and tightly-coupled scheme in a GNSS-degraded environment," *IEEE Sensors J.*, vol. 20, no. 6, pp. 3057–3069, Mar. 2020.

[14] J. Fritsch, T. Kühnl, and F. Kummert, "Monocular road terrain detection by combining visual and spatial information," *IEEE Trans. Intell. Transp. Syst.*, vol. 15, no. 4, pp. 1586–1596, Aug. 2014.

[15] J. Engel, T. Schöps, and D. Cremers, "LSD-SLAM: Large-scale direct monocular SLAM," in *Proc. Eur. Conf. Comput. Vis.* Berlin, Germany: Springer, 2014, pp. 834–849.

[16] C. Zhang, T. Huang, R. Zhang, and X. Yi, "PLD-SLAM: A new RGB-D SLAM method with point and line features for indoor dynamic scene," *ISPRS Int. J. Geo-Inf.*, vol. 10, no. 3, p. 163, Mar. 2021.

[17] M. C. Bakkay, M. Arafa, and E. Zagrouba, "Dense 3D SLAM in dynamic scenes using Kinect," in *Proc. Iberian Conf. Pattern Recognit. Image Anal.* Berlin, Germany: Springer, 2015, pp. 121–129.

[18] Y. Ma, Y. Chen, L. Zhang, Z. Zhang, J. Wang, W. Yu, Z. Xing, Y. Hu, and Z. Liu, "Three-dimensional reconstruction of plants and a single building from UAV images," *Int. J. Precis. Agricult. Aviation*, vol. 1, no. 1, pp. 80–88, 2018.

[19] Z. Zheng, X. Li, Z. Sun, and X. Song, "A novel visual measurement framework for land vehicle positioning based on multimodule cascaded deep neural network," *IEEE Trans. Ind. Informat.*, vol. 17, no. 4, pp. 2347–2356, Apr. 2021.

[20] D. Xu, Q. Jia, P. Ye, and H. Sun, "A visual relocation algorithm with illumination changing robustness," in *Proc. 6th Int. Conf. Syst. Informat. (ICSAI)*, Nov. 2019, pp. 127–132.

[21] Y. Lan, L. Geng, W. Li, W. Ran, X. Yin, and L. Yi, "Development of a robot with 3D perception for accurate row following in vineyard," *Int. J. Precis. Agricult. Aviation*, vol. 1, no. 1, pp. 14–21, 2018.

[22] T. Ran, L. Yuan, J. Zhang, D. Tang, and L. He, "RS-SLAM: A robust semantic SLAM in dynamic environments based on RGB-D sensor," *IEEE Sensors J.*, vol. 21, no. 18, pp. 20657–20664, Sep. 2021.

[23] Z. Zhu and C. Taylor, "Conservative uncertainty estimation in map-based vision-aided navigation," *IEEE Trans. Aerosp. Electron. Syst.*, vol. 53, no. 2, pp. 941–949, Apr. 2017.

[24] X. Mu, Y. Liu, L. Guo, J. Lin, and R. Schober, "Intelligent reflecting surface enhanced indoor robot path planning: A radio map-based approach," *IEEE Trans. Wireless Commun.*, vol. 20, no. 7, pp. 4732–4747, Jul. 2021.

[25] G. Wan, X. Yang, R. Cai, H. Li, Y. Zhou, H. Wang, and S. Song, "Robust and precise vehicle localization based on multi-sensor fusion in diverse city scenes," in *Proc. IEEE Int. Conf. Robot. Autom. (ICRA)*, May 2018, pp. 4670–4677.

[26] R. A. Newcombe, S. J. Lovegrove, and A. J. Davison, "DTAM: Dense tracking and mapping in real-time," in *Proc. Int. Conf. Comput. Vis.*, Nov. 2011, pp. 2320–2327.

[27] C. Forster, M. Pizzoli, and D. Scaramuzza, "SVO: Fast semi-direct monocular visual odometry," in *Proc. IEEE Int. Conf. Robot. Autom. (ICRA)*, May 2014, pp. 15–22.

[28] R. Mur-Artal and J. D. Tardós, "ORB-SLAM2: An open-source SLAM system for monocular, stereo, and RGB-D cameras," *IEEE Trans. Robot.*, vol. 33, no. 5, pp. 1255–1262, Oct. 2017.

[29] Z. Zhao, W. Zhang, J. Gu, J. Yang, and K. Huang, "LiDAR mapping optimization based on lightweight semantic segmentation," *IEEE Trans. Intell. Vehicles*, vol. 4, no. 3, pp. 353–362, Sep. 2019.

[30] J. Zhang and S. Singh, "Loam: LiDAR odometry and mapping in real-time," in *Proc. Robot., Sci. Syst.*, vol. 2, no. 9, Berkeley, CA, USA, 2014, pp. 1–9.

[31] S. Anderson and T. D. Barfoot, "RANSAC for motion-distorted 3D visual sensors," in *Proc. IEEE/RSJ Int. Conf. Intell. Robots Syst.*, Nov. 2013, pp. 2093–2099.

[32] C. H. Tong and T. D. Barfoot, "Gaussian process Gauss–Newton for 3D laser-based visual odometry," in *Proc. IEEE Int. Conf. Robot. Autom.*, May 2013, pp. 5204–5211.

[33] Q. Deng, H. Sun, F. Chen, Y. Shu, H. Wang, and Y. Ha, "An optimized FPGA-based real-time NDT for 3D-LiDAR localization in smart vehicles," *IEEE Trans. Circuits Syst. II, Exp. Briefs*, vol. 68, no. 9, pp. 3167–3171, Sep. 2021.

[34] S. Srinara, C.-M. Lee, S. Tsai, G.-J. Tsai, and K.-W. Chiang, "Performance analysis of 3D NDT scan matching for autonomous vehicles using INS/GNSS/3D LiDAR-SLAM integration scheme," in *Proc. IEEE Int. Symp. Inertial Sensors Syst. (INERTIAL)*, Mar. 2021, pp. 1–4.

[35] Z. Zhou, C. Zhao, D. Adolfsson, S. Su, Y. Gao, T. Duckett, and L. Sun, "NDT-transformer: Large-scale 3D point cloud localisation using the normal distribution transform representation," in *Proc. IEEE Int. Conf. Robot. Autom. (ICRA)*, May 2021, pp. 5654–5660.
[36] S. Chen, H. Ma, C. Jiang, B. Zhou, W. Xue, Z. Xiao, and Q. Li, "NDT-LOAM: A real-time LiDAR odometry and mapping with weighted NDT and LFA," *IEEE Sensors J.*, vol. 22, no. 4, pp. 3660–3671, Feb. 2022.
[37] Y.-C. Kan, L.-T. Hsu, and E. Chung, "Performance evaluation on map-based NDT scan matching localization using simulated occlusion datasets," *IEEE Sensors Lett.*, vol. 5, no. 3, pp. 1–4, Mar. 2021.
[38] A. Gellert, D. Sarbu, S.-A. Precup, A. Matei, D. Circa, and C.-B. Zamfirescu, "Estimation of missing LiDAR data for accurate AGV localization," *IEEE Access*, vol. 10, pp. 68416–68428, 2022.
[39] C. Kim, S. Cho, M. Sunwoo, P. Resende, B. Bradai, and K. Jo, "A geodetic normal distribution map for long-term LiDAR localization on earth," *IEEE Access*, vol. 9, pp. 470–484, 2021.
[40] Z. Vincze, A. Rövid, and V. Tihanyi, "Automatic label injection into local infrastructure LiDAR point cloud for training data set generation," *IEEE Access*, vol. 10, pp. 91213–91226, 2022.
[41] N. M. Singer and V. K. Asari, "DALES objects: A large scale benchmark dataset for instance segmentation in aerial LiDAR," *IEEE Access*, vol. 9, pp. 97495–97504, 2021.
[42] Y. Wang and X. Xie, "Dynamic simulation of noise in 3D infrared scene simulation," in *Proc. Int. Conf. Netw. Inf. Syst. Comput.*, Jan. 2015, pp. 251–254.
[43] J. Zhu, D. Dai, W. Wu, X. Wang, and J. Wang, "Assessment of the impact of the measurement noise on the gravity anomaly matching technique," in *Proc. 26th Saint Petersburg Int. Conf. Integr. Navigat. Syst. (ICINS)*, May 2019, pp. 1–3.
[44] P. A. Stavrou and M. Skoglund, "New formulation and computation of NRDF for time-varying multivariate Gaussian processes with correlated noise," *IEEE Control Syst. Lett.*, vol. 6, pp. 331–336, 2022.
[45] G. Kermarrec, A. Jain, and S. Schön, "Kalman filter and correlated measurement noise: The variance inflation factor," *IEEE Trans. Aerosp. Electron. Syst.*, vol. 58, no. 2, pp. 766–780, Apr. 2022.
[46] V. M. Artyushenko and V. I. Volovach, "Using the poly-Gaussian models to represent non-Gaussian signals and noises," in *Proc. Syst. Signals Generating Process. Field Board Commun.*, Mar. 2022, pp. 1–5.
[47] S. Kong, F. Shi, C. Wang, and C. Xu, "Point cloud generation from multiple angles of voxel grids," *IEEE Access*, vol. 7, pp. 160436–160448, 2019.
[48] T. Oblak, J. Šircelj, V. Štruc, P. Peer, F. Solina, and A. Jaklič, "Learning to predict superquadric parameters from depth images with explicit and implicit supervision," *IEEE Access*, vol. 9, pp. 1087–1102, 2021.
[49] X. Wang, H. Shang, and L. Jiang, "Improved point pair feature based cloud registration on visibility and downsampling," in *Proc. Int. Conf. Netw. Syst. AI (INSAI)*, Nov. 2021, pp. 82–89.
[50] D. Yang and B. Jiabao, "An optimization method for video upsampling and downsampling using interpolation-dependent image downsampling," in *Proc. 4th Int. Conf. Inf. Commun. Signal Process. (ICICSP)*, Sep. 2021, pp. 438–442.
[51] O. Hirose, "Acceleration of non-rigid point set registration with downsampling and Gaussian process regression," *IEEE Trans. Pattern Anal. Mach. Intell.*, vol. 43, no. 8, pp. 2858–2865, Aug. 2021.
[52] B. Zou, H. Qiu, and Y. Lu, "Point cloud reduction and denoising based on optimized downsampling and bilateral filtering," *IEEE Access*, vol. 8, pp. 136316–136326, 2020.

JIAN GU received the B.S. degree in mechanical design and manufacturing and automation from the Yancheng Institute of Technology, in 2019. He is currently pursuing the master's degree with the Shandong University of Technology. His research interests include mobile robots, SLAM, and repositioning.

YUBIN LAN received the B.S. and Ph.D. degrees in agricultural machinery engineering from Jilin University, in 1982 and 1989, respectively, and the second Ph.D. degree in agricultural engineering from Texas A&M University, in 1993. His main research interests include remote sensing technology and precision agriculture. He is the Director and the Chief Scientist at the National Center for International Collaboration Research on Precision Agricultural Aviation Pesticides Spraying Technology (NPAAC), China. He has been engaged in agricultural engineering over 40 years. He firstly proposed the concept "Precision Agricultural Aviation (PAA)" in the world and has established the first "Ecological Unmanned Farm" in China. He is currently the Chairperson of the International Society of Precision Agricultural Aviation (ISPAA) and the CIGR Precision Aerial Application Technology Working Group. He is a well-known scientist in agricultural aviation, especially in agricultural drones' research and applications.

FANXIA KONG received the B.S. degree in mechanical design and manufacturing from Shandong Engineering College, in 2000, the M.S. degree in agricultural mechanization engineering from the Shandong University of Technology, in 2005, and the Ph.D. degree in mechanical manufacturing and its automation from the Beijing University of Aeronautics and Astronautics, in 2010. She is currently working as an Associate Professor at the Shandong University of Technology. Her main research interests include industrial design and intelligent agricultural equipment manufacturing.

LEI LIU received the B.S. degree from the Department of Mechanical and Electronic Engineering, Shandong University of Technology, in 2022, where he is currently pursuing the M.S. degree in agricultural equipment engineering. His research interests include agricultural machinery and embedded operating systems.

LILI YI received the B.S. degree in applied physics from China Agricultural University, in 2004, the M.S. degree in detection technology and automatic equipment from Beihang University, in 2007, and the Ph.D. degree from Nanyang Technological University, Singapore, in 2015. Since 2018, she has been an Associate Professor with the Shandong University of Technology. Her main research interests include geolocation and autonomous navigation.